Research Square

Preprints are preliminary reports that have not undergone peer review.
They should not be considered conclusive, used to inform clinical practice,
or referenced by the media as validated information.

# Deep Learning Reconstruction for Low-Dose Dual-Energy CT Pulmonary Angiography: Optimization of Energy Levels and Assessment of Subsegmental Arteries

**Dapeng Zhang**
the Affiliated Hospital of Xuzhou Medical University
**Zhen Wang**
the Affiliated Hospital of Xuzhou Medical University
**Zhongxiao Liu**
the Affiliated Hospital of Xuzhou Medical University
**Juan Long**
the Affiliated Hospital of Xuzhou Medical University
**Hongfei Xia**
the Affiliated Hospital of Xuzhou Medical University
**Shenman Qiu**
the Affiliated Hospital of Xuzhou Medical University
**Xiaonan Sun**
the Affiliated Hospital of Xuzhou Medical University
**Bo Sun**
the Affiliated Hospital of Xuzhou Medical University
**Chong Meng**
the Affiliated Hospital of Xuzhou Medical University
**Aiyun Sun**
GE HealthCare China
**Chunfeng Hu**
the Affiliated Hospital of Xuzhou Medical University
**Kai Xu**
the Affiliated Hospital of Xuzhou Medical University
**Yankai Meng**
mengyankai@126.com

the Affiliated Hospital of Xuzhou Medical University

**Article**

**Keywords:** Pulmonary Embolism, CT Angiography, Dual-Energy CT, Deep Learning, Image Reconstruction, Radiation Dosage

**Posted Date:** August 20th, 2026

**DOI:** https://doi.org/10.21203/rs.3.rs-10262111/v1

**License:** This work is licensed under a Creative Commons Attribution 4.0 International License. Read Full License

**Additional Declarations:** No competing interests reported.

# Deep Learning Reconstruction for Low-Dose Dual-Energy CT Pulmonary Angiography: Optimization of Energy Levels and Assessment of Subsegmental Arteries

Dapeng Zhang, MS, [1,2,3#] Zhen Wang, MS, [1,2,3#] Zhongxiao Liu, MS, [1,2,3#] Juan Long, MS, [1,2,3] Hongfei Xia, MS, [1,2,3] Shenman Qiu, MS, [1,2,3] Xiaonan Sun, MS, [1,2,3] Bo Sun, MS, [1,2,3] Chong Meng, MS, [1,2,3] Aiyun Sun, PhD, [4] Chunfeng Hu, MD, [1,2,3] Kai Xu, MD, [1,2,3] Yankai Meng, MD, [1,2,3*]

1 Department of Radiology, the Affiliated Hospital of Xuzhou Medical University, Xuzhou, Jiangsu, 221002, China

2 School of Medical Imaging, Xuzhou Medical University, Xuzhou, Jiangsu, 221002, China

3 Jiangsu Provincial Engineering Research Center for Medical Imaging and Digital Medicine, Xuzhou, Jiangsu, 221002, China

4 CT Imaging Research Center, GE HealthCare China, Shanghai, China

**Note:** Dapeng Zhang[#] Zhen Wang[#] and Zhongxiao Liu[#] contributed equally to this article.

***Corresponding Author:**

Yankai Meng

Department of Radiology, the Affiliated Hospital of Xuzhou Medical University

School of Medical Imaging, Xuzhou Medical University

Jiangsu Provincial Engineering Research Center for Medical Imaging and Digital Medicine

Email: mengyankai@126.com

ORCID: https://orcid.org/0000-0002-9671-538X

## Authorship and contributions:

Conception of the work: Yankai Meng, Kai Xu, and Dapeng Zhang.

Design of the work: Yankai Meng, Kai Xu, Chunfeng Hu, Dapeng Zhang, and Aiyun Sun.

Acquisition of data for the work: Zhongxiao Liu, Shenman Qiu, Xiaonan Sun, Hongfei Xia, Bo Sun, Chong Meng, and Zhen Wang.

Analysis of data for the work: Yankai Meng, Hongfei Xia, Shenman Qiu,Juan Long, Dapeng Zhang, and Zhen Wang.

Interpretation of data for the work: Yankai Meng, Kai Xu,Shenman Qiu, and Dapeng Zhang.

Drafting the work: Yankai Meng, Kai Xu, Dapeng Zhang, Zhen Wang, and Juan Long.

Revising the work critically for important intellectual content: Yankai Meng, Kai Xu, Chunfeng Hu, Dapeng Zhang, and Aiyun Sun.

Agreement to be accountable for all aspects of the work in ensuring that questions related to the accuracy or integrity of any part of the work are appropriately investigated and resolved: **Yankai Meng**.

## Conflict of interest declaration:

There are no conflicts of interest to declare.

## Data availability statement

The datasets generated and/or analyzed during the current study are not publicly available due to patient privacy protection and ethical restrictions regarding the sharing of individual medical imaging data. The datasets may contain potentially identifiable clinical and imaging information; therefore, they cannot be deposited in a public repository. However, de-identified data that support the findings of this study are available from the corresponding author upon reasonable request and subject to approval by the institutional ethics committee.

## Grant support

This study was funded by the Special Fund for Overseas Training of Employees of the Affiliated Hospital of Xuzhou Medical University;Project supported by the Affiliated Hospital of Xuzhou Medical University（2025ZL07）.

## Acknowledgment

We acknowledge financial support from the Special Fund for Overseas Training of Employees of the Affiliated Hospital of Xuzhou Medical University.

**Word count:** 4865 words (4 figures, 4 tables, 3 supplementary tables and 4 supplementary figure)

**Conflicts of interest statement:** There are no conflicts of interest to declare.

**Running title:** 40 keV DLIR for Low-Dose DE-CTPA

**Keywords:** Pulmonary Embolism; CT Angiography; Dual-Energy CT; Deep Learning; Image Reconstruction; Radiation Dosage.

## Abbreviation index

**ASIR-V:** adaptive statistical iterative reconstruction-V

**BMI:** body mass index

**CI:** confidence interval

**CNR:** contrast-to-noise ratio

**$CTDI_{vol}$:** volume CT dose index

**DE-CTPA:** dual-energy CT pulmonary angiography

**DLIR:** deep learning image reconstruction

**DLIR-H:** deep learning image reconstruction, high strength

**DLIR-M:** deep learning image reconstruction, medium strength

**DLP:** dose-length product

**ED:** effective dose

**GSI:** Gemstone Spectral Imaging

**HU:** Hounsfield unit

**ICC:** intraclass correlation coefficient

**keV:** kiloelectron volt

**LPA:** left pulmonary artery

**NI:** noise index

**PA:** pulmonary artery (main)

**PE:** pulmonary embolism

**ROI:** region of interest

**RPA:** right pulmonary artery

**SD:** standard deviation

**SNR:** signal-to-noise ratio

**VMI:** virtual monoenergetic imaging

**Acknowledgments:** We acknowledge financial support from the Special Fund for Overseas Training of Employees of the Affiliated Hospital of Xuzhou Medical University.

**Funding:** This study was funded by the Special Fund for Overseas Training of Employees of the Affiliated Hospital of Xuzhou Medical University; Project supported by the Affiliated Hospital of Xuzhou Medical University（2025ZL07）.

**Ethics declarations:**

This prospective study was conducted between January and August 2025 and was approved by the Institutional Review Board of the Affiliated Hospital of Xuzhou Medical University (Approval No. XYFY2025-KL572-01). All methods were performed in accordance with the relevant guidelines and regulations, including the Declaration of Helsinki. Written informed consent was obtained from all patient participants. Informed consent was also obtained from the participating radiologist.

***Corresponding Author:**

Yankai Meng, Department of Radiology, the Affiliated Hospital of Xuzhou Medical

University; School of Medical Imaging, Xuzhou Medical University; Jiangsu Provincial Engineering Research Center for Medical Imaging and Digital Medicine

Email: mengyankai@126.com

**Corresponding Author Statement:**

Yankai Meng is designated as the corresponding author for this article. He will be responsible for handling all correspondence throughout the refereeing process, publication process, and post-publication. This includes addressing any future inquiries regarding the results, data, methodology, and materials presented in this work.

**Abstract**

**Background:** Dual-energy CT pulmonary angiography (DE-CTPA) facilitates dose reduction through virtual monoenergetic imaging (VMI). However, the optimal reconstruction strategy for balancing image noise and vascular contrast in low-dose protocols—particularly for evaluating subsegmental arteries—remains to be fully established.

**Purpose:** To determine the optimal VMI energy level and reconstruction algorithm for "double-low" (low radiation and contrast media) DE-CTPA and to compare the image quality of deep learning image reconstruction (DLIR) versus

adaptive statistical iterative reconstruction-V (ASIR-V) in patients with pulmonary embolism (PE).

**Materials and Methods:** This study, conducted between January and August 2025, included 39 patients with suspected PE who underwent DE-CTPA using an optimized low-dose protocol. Images were reconstructed at VMI levels from 40 to 140 keV using ASIR-V (30%–70%) and DLIR (medium [DLIR-M] and high [DLIR-H] strength). Objective metrics (CT attenuation, image noise, signal-to-noise ratio [SNR], and contrast-to-noise ratio [CNR]) were evaluated in the main, lobar, segmental, and subsegmental pulmonary arteries. Subjective image quality was assessed by two radiologists using a 5-point Likert scale.

**Results:** Among all energy levels, 40 keV VMI yielded the highest vascular attenuation. At this energy level, DLIR-H achieved significantly lower image noise compared with ASIR-V and DLIR-M ($P < 0.05$). The 40 keV DLIR-H protocol demonstrated the highest CNR across all vascular territories, significantly outperforming the standard 70 keV ASIR-V 50% protocol in the pulmonary trunk ($P = 0.013$), lobar ($P < 0.001$), segmental ($P = 0.010$), and subsegmental arteries ($P < 0.001$). Subjectively, 40 keV DLIR-H images were rated as excellent (median score, 5.0) and were noninferior to the standard 70 keV protocol for evaluating segmental and subsegmental arteries ($P > 0.05$).

**Conclusion:** A low-dose DE-CTPA protocol combining 40 keV VMI with high-strength DLIR provides superior objective image quality and excellent

subjective depiction of subsegmental arteries while substantially reducing radiation and contrast media exposure.

## Introduction

Pulmonary embolism (PE) is a leading cause of cardiovascular mortality, necessitating timely and accurate diagnosis[1]. While CT pulmonary angiography (CTPA) is the reference standard, the visualization of peripheral emboli—particularly in segmental and subsegmental arteries—remains challenging due to limited vascular enhancement and respiratory motion artifacts[2]. Furthermore, the increasing utilization of CTPA raises concerns regarding cumulative radiation exposure and contrast-induced nephropathy (CIN), driving the clinical demand for "double-low" protocols (reduced radiation and contrast media)[3].

Dual-energy CT (DECT) addresses these challenges through virtual monoenergetic imaging (VMI)[4]. By reconstructing images at low energy levels (e.g., 40–50 keV), DECT significantly boosts the attenuation of iodinated contrast, theoretically allowing for substantial reductions in contrast medium volume without compromising vascular opacity[5]. However, a major limitation of low keV imaging is the exponential increase in image noise, which can degrade image quality and obscure subtle emboli. Consequently, a consensus regarding the optimal energy level that balances vascular contrast and image noise has yet to be established[6].

Traditional noise reduction techniques, such as adaptive statistical iterative reconstruction (ASIR-V), are effective but often compromise image texture and spatial resolution, imparting a characteristic "waxy" appearance that may affect diagnostic confidence in small vessels[7]. Recently, Deep Learning Image Reconstruction (DLIR) algorithms have been developed to overcome these trade-offs. Trained on high-quality filtered back-projection (FBP) data, DLIR aims to suppress noise while preserving anatomical texture and spatial resolution[8]. While DLIR has shown promise in standard CT protocols, its specific performance in handling the extreme noise inherent to 40 keV VMI—especially within the distal subsegmental pulmonary vasculature—remains under-investigated.

We hypothesized that high-strength DLIR (DLIR-H) could effectively mitigate the noise penalty of 40 keV VMI, enabling a high-quality, ultra-low-contrast DE-CTPA protocol. Therefore, the purpose of this study was to determine the optimal VMI energy level and reconstruction algorithm for "double-low" DE-CTPA and to evaluate the objective and subjective image quality across the pulmonary arterial tree, with specific attention to segmental and subsegmental arteries in patients with PE.

## Materials and Methods

### Study Population

This prospective study was conducted between January and August 2025 and was approved by the Institutional Review Board of the Affiliated Hospital of Xuzhou Medical University (Approval No. XYFY2025-KL572-01). All methods were performed in accordance with the relevant guidelines and regulations, including the Declaration of Helsinki. Written informed consent was obtained from all participants.

The study enrolled adult patients with clinically suspected pulmonary embolism (PE) who underwent DE-CTPA. Inclusion criteria were: (a) clinical indication for CTPA; and (b) confirmed diagnosis of PE requiring thrombolytic therapy with subsequent follow-up imaging. Exclusion criteria were: (a) history of severe allergic reaction to iodinated contrast media; (b) severe cardiac, hepatic, or renal dysfunction (defined as eGFR < 30 mL/min/1.73 $m^2$); (c) untreated hyperthyroidism; or (d) inability to cooperate with breath-holding instructions. A flowchart of patient enrollment is presented in **Figure 1**.

## CT Acquisition Protocol

All examinations were performed on a 256-slice DECT scanner (Revolution CT; GE Healthcare, Milwaukee, WI, USA) in spectral imaging mode (Gemstone Spectral Imaging [GSI]). Patients were scanned in the supine position from the thoracic inlet to the costophrenic angle.

A low-contrast protocol was employed using 350 mgI/mL iodixanol (Hengrui Pharmaceutical, Lianyungang, China). Contrast media was administered via a

dual-head power injector (CT Motion-XD8000; Ulrich Medical, Erlangen, Germany) at a dose of 0.4 mL/kg and a flow rate of 4.25 mL/s (mean), followed by a 30-mL saline flush. Bolus tracking was used with a region of interest (ROI) placed in the main pulmonary artery and a trigger threshold of 50 HU.

Acquisition parameters were as follows: fast kVp switching between 80 and 140 kVp; GSI Assist modulated tube current (reference, 320 mA); rotation time, 0.28 seconds; pitch, 0.992:1; and Noise Index, 10. The detector configuration was 128 × 0.625 mm. The volume CT dose index ($CTDI_{vol}$) and dose-length product (DLP) were recorded from the dose report. Effective dose (ED) was calculated as DLP × $k$, using a conversion coefficient ($k$) of 0.014 $mSv \cdot mGy^{-1} \cdot cm^{-1}$.

## Image Reconstruction

Raw spectral data were processed on a dedicated workstation (AW Server 4.7; GE Healthcare). Virtual monoenergetic images (VMI) were reconstructed at **40 keV** (target energy) and **70 keV** (standard reference) with a slice thickness and interval of 1.25 mm and 0.625 mm, respectively.

Images were reconstructed using two algorithms:

**Adaptive Statistical Iterative Reconstruction-V (ASIR-V):** Reconstructed at 30%, 50%, and 70% blending levels.

**Deep Learning Image Reconstruction (DLIR):** A commercial deep convolutional neural network-based algorithm (TrueFidelity, GE Healthcare) was applied at medium (DLIR-M) and high (DLIR-H) strength settings[9].

For the purpose of this study, the **70 keV ASIR-V 50%** reconstruction served as the standard control group.

## Quantitative Image Analysis

Quantitative assessment was performed by a radiologist (XX, with 3 years of experience) who was blinded to the reconstruction protocols. ROIs were placed in the main, left, and right pulmonary arteries, and the paraspinal musculature (infraspinatus muscle) at the level of the pulmonary bifurcation. ROIs were drawn as large as possible (covering ~2/3 of the vessel lumen) while strictly avoiding vessel walls, calcifications, and artifacts.

For patients with confirmed PE, additional ROIs were placed within the embolus and the adjacent contrast-enhanced vessel lumen.

Image quality metrics were calculated as follows:

**CT Attenuation:** Mean Hounsfield unit (HU) within the vascular ROI.

**Image Noise:** Standard deviation (SD) of the HU within the vascular ROI.

**Signal-to-Noise Ratio (SNR):**

$$SNR = \frac{CTvessel}{Noisevessel}$$

Contrast-to-Noise Ratio (CNR):

$$CNR = \frac{CTvessel - CTmuscle}{Noisevessel}$$

Embolus-Specific CNR (CNRPE):

$$CNR_{PE} = \frac{CTvessel - CTembolus}{Noiseembolus}$$

Where *CTvessel* is the attenuation of the contrast-filled lumen, *CTembolus* is the attenuation of the thrombus, and *Noiseembolus* is the SD within the thrombus ROI.

## Qualitative Image Analysis

Subjective image quality was independently evaluated by two radiologists (XXX and XX, with 15 and 30 years of experience, respectively) using a double-blinded approach. The radiologists involved in image assessment were members of the research team and did not undergo any study-related interventions; therefore, informed consent was not applicable.

Images were reviewed on a diagnostic monitor (JUSHA-C42E; Nanjing Jusha Display Technology) with preset window settings (width, 400 HU; level, 60 HU), which readers were allowed to adjust.

A 5-point Likert scale was used to assess four parameters: image noise, vascular edge clarity, noise texture, and overall diagnostic confidence (**Table E1**). For PE-positive cases, specific attention was paid to the delineation of the embolus borders. In cases of disagreement, a consensus was reached through discussion.

### Statistical Analysis

Statistical analyses were performed using SPSS software (version 27.0; IBM). Normality was assessed using the Shapiro-Wilk test. Continuous variables are expressed as means ± standard deviations (normally distributed) or medians with interquartile ranges (non-normally distributed).

Comparison of quantitative and qualitative metrics across reconstruction algorithms was performed using repeated-measures analysis of variance (ANOVA) with LSD post-hoc tests (for normal data) or the Friedman test with Dunn's post-hoc tests (for non-normal data). Interreader agreement was evaluated using the intraclass correlation coefficient (ICC) (estimates: <0.5, poor; 0.5–0.75, moderate; 0.75–0.9, good; >0.9, excellent). A two-sided *P* value < .05 was considered statistically significant.

## Results

### Patient Demographics

The final study cohort consisted of 39 patients (19 men [48.7%] and 20 women [51.3%]), with a median age of 73 years (interquartile range [IQR]: 60–77 years). The mean BMI was 23.8 kg/m $^2$ ± 4.3. The protocol achieved a low radiation and contrast burden: the median ED was 3.0 mSv (IQR: 2.5–4.0 mSv), and the mean total contrast volume was 25.6 mL ± 5.3 (**Table 1**).

### Optimization of Energy Level

Vascular attenuation demonstrated a progressive decline from 40 keV to 140 keV (**Figure E1**). While image noise was inversely related to energy levels (peaking at 40 keV), the reconstruction algorithm significantly influenced the noise floor. Across the entire 40–140 keV spectrum, DLIR-H consistently yielded the lowest image noise, whereas ASIR-V 30% exhibited the highest. Consequently, the combination of 40 keV and DLIR-H achieved the highest SNR and CNR values, outperforming all other energy-algorithm combinations (**Figure 2**). Based on these findings, 40 keV datasets were selected for detailed anatomical analysis.

**Findings:** Shaded areas represent 95% confidence intervals. Note that while SNR and CNR generally decline as energy levels increase (due to reduced iodine attenuation), the **40 keV DLIR-H** protocol (purple line) consistently achieves the highest values across all three vascular territories, effectively suppressing the quantum noise inherent to low-energy imaging.

Findings:

(A) Vascular attenuation increases substantially at lower keV levels (peaking at 40 keV), independent of the reconstruction algorithm used.

(B) While image noise naturally increases at lower energies, the DLIR-H algorithm (purple line) maintains the lowest noise floor at 40 keV compared with ASIR-V and DLIR-M, enabling the high SNR/CNR observed in Figure 2.

## Objective Image Quality of PE-Affected Vessels

Quantitative assessment revealed significant improvements in image quality with the proposed protocol (Tables 2, Table E2, and Figure 3).

### CT Attenuation and Noise:

As shown in Table 2, all 40 keV algorithms demonstrated substantially higher vascular attenuation (mean range: 148–186 HU) compared to the 70 keV control (mean range: 60–79 HU). While lower energy levels typically increase noise, the 40 keV DLIR-H protocol achieved the lowest standard deviation among the 40 keV groups. Pairwise comparisons (Table E2) confirmed that noise levels in 40 keV DLIR-H were significantly lower than those in 40 keV ASIR-V 50% across the lobar ($P$ = 0.006), segmental ($P$ = 0.014), and subsegmental arteries ($P$ = 0.031).

### Contrast-to-Noise Ratio (CNR):

Consequently, the 40 keV DLIR-H protocol yielded the highest CNR across all vascular levels (Table 2). Specifically, it provided significantly higher CNR

compared to the standard 70 keV ASIR-V protocol in the pulmonary trunk ($P$ = 0.013), lobar ($P$ < 0.001), segmental ($P$ = 0.010), and subsegmental arteries ($P$ < 0.001; **Table E2**). Notably, for the visualization of subsegmental emboli, DLIR-H outperformed both the standard control and the 40 keV ASIR-V 50% protocol ($P$ = 0.045), underscoring its value in depicting peripheral vasculature.

**Findings:** Note that while all 40 keV protocols show improvement over the standard 70 keV control (red box), the **40 keV DLIR-H protocol (purple box)** consistently yields the highest median CNR with a narrow IQR, indicating both superior image quality and high stability, particularly in the distal segmental and subsegmental vessels.

**Findings:** As expected based on the k-edge of iodine, all 40 keV reconstruction groups (blue, green, and purple boxes) demonstrate substantially higher attenuation values compared with the standard 70 keV control (red box). Note that at the fixed energy level of 40 keV, the choice of reconstruction algorithm (ASIR-V vs. DLIR) has a negligible impact on the mean CT attenuation (**Figure E2**).

**Findings:** Lowering the energy level to 40 keV inherently increases quantum noise, as seen in the significantly higher noise levels of the 40 keV ASIR-V 50% group (blue box). However, the **40 keV DLIR-H algorithm (purple box)** effectively suppresses this noise penalty, achieving noise levels comparable to—and in distal vessels, often lower than—the standard 70 keV ASIR-V protocol (red box) (**Figure E3**).

**Findings:** Driven by the dual benefits of increased iodine attenuation (from 40 keV) and advanced noise suppression (from Deep Learning), the **40 keV DLIR-H protocol (purple box)** achieves the highest SNR across all vascular territories, significantly outperforming both the standard control and the 40 keV ASIR-V protocol (**Figure E4**).

### Interreader Agreement

Interreader agreement for subjective image quality assessment was excellent across all pulmonary vascular regions. The intraclass correlation coefficients (ICCs) for all qualitative parameters (image noise, edge clarity, noise texture, and spatial resolution) ranged from 0.847 to 0.982, indicating high consistency between the two radiologists (**Table E3**).

### Subjective Image Quality Assessment

Subjective image quality scores for the 40 keV DLIR-H protocol were consistently rated as excellent (median score: 5.00) across all pulmonary vascular territories, from the pulmonary trunk to the subsegmental arteries (**Table 3**).

### Comparison with Standard Dose (70 keV):

Despite the lower radiation and contrast dose, the 40 keV DLIR-H images demonstrated diagnostic quality comparable to the standard 70 keV ASIR-V 50% protocol. Post-hoc analyses (**Table 4**) revealed no statistically significant differences between these two groups in terms of image noise, edge clarity,

noise texture, or spatial resolution across the majority of vascular segments (P3 > 0.050 for all).

**Comparison within Low-Dose (40 keV) Algorithms:**

Among the 40 keV reconstructions, the reconstruction algorithm significantly impacted image quality. The DLIR-H algorithm significantly outperformed both ASIR-V 50% and DLIR-M. Specifically, in the **segmental and subsegmental arteries**, DLIR-H yielded significantly higher scores for image noise suppression, edge clarity, and noise texture compared to 40 keV ASIR-V 50% (P5 < 0.001 for all). Furthermore, DLIR-H demonstrated superior noise texture and spatial resolution compared to DLIR-M in distal vessels (P6 < 0.050; **Table 4**), confirming its superiority in depicting fine vascular details in low-energy datasets.

**Findings:** While all 40 keV images demonstrate substantially higher vascular attenuation compared with the 70 keV control, the **40 keV DLIR-H** reconstruction (far right column) significantly suppresses the image noise inherent to low-energy imaging. Consequently, it provides the best embolus conspicuity and sharpest vascular edges, particularly in the segmental and subsegmental arteries (Rows C and D)(**Figure 4**).

## Discussion

The primary finding of this prospective study is that the combination of 40 keV VMI and DLIR-H establishes a robust "double-low" DE-CTPA protocol. We

demonstrated that this strategy yields superior objective image quality metrics—specifically SNR and CNR—across the entire pulmonary vasculature compared to the standard 70 keV ASIR-V protocol. Crucially, in the challenging segmental and subsegmental arteries, 40 keV DLIR-H maintained excellent subjective image quality that was comparable to the standard dose protocol, despite a substantial reduction in contrast medium volume (~26 mL) and radiation dose.

Our results address the ongoing debate regarding the optimal energy level for pulmonary angiography. While previous studies have established that lower keV settings (40–50 keV) dramatically increase iodine attenuation[10], the clinical adoption of these ultra-low energy levels has been hindered by excessive quantum noise[11]. Traditional iterative reconstruction algorithms, such as ASIR-V, often fail to adequately suppress this noise without creating a "waxy" texture that obscures fine vascular details[12]. Our data confirm this limitation; 40 keV images reconstructed with ASIR-V exhibited significantly lower subjective scores than the control group. In contrast, DLIR-H effectively decoupled the trade-off between noise reduction and spatial resolution. By leveraging deep neural networks trained on high-fidelity data, DLIR-H restored the texture and edge sharpness of the 40 keV images, rendering them diagnostically equivalent to standard 70 keV images but with the added benefit of higher vascular contrast[13].

The improved visualization of subsegmental arteries observed in our study has significant clinical implications. The diagnosis of subsegmental pulmonary embolism (SSPE) remains a gray area in clinical practice, often plagued by high inter-reader variability and equivocal findings[14]. Missed SSPE can lead to recurrence or chronic thromboembolic pulmonary hypertension, particularly in high-risk oncology patients[15]. We found that 40 keV DLIR-H provided the highest CNR and edge clarity in distal vessels. This enhanced conspicuity may increase diagnostic confidence for peripheral emboli, potentially reducing the rate of indeterminate examinations. While our study focused on image quality rather than diagnostic accuracy, the superior CNR suggests a potential for improved sensitivity in detecting small-vessel PE.

Furthermore, this protocol aligns with the ALARA (As Low As Reasonably Achievable) principle and nephroprotection strategies[16]. The mean contrast volume in our cohort was approximately 26 mL, which is significantly lower than the 50–100 mL typically used in routine CTPA[17]. This reduction is particularly advantageous for elderly patients and those with pre-existing renal insufficiency, a demographic frequently suspected of having PE[18]. Additionally, the median effective dose was reduced to approximately 3 mSv, comparing favorably to the 5–10 mSv reported in conventional CTPA studies[19].

Our study had limitations. First, it was a single-center study with a relatively small sample size, which may limit generalizability. Second, we evaluated a specific

vendor's DECT platform and proprietary DLIR algorithm; results may vary with other manufacturers. Third, because the study design focused on image quality optimization in patients with confirmed PE, we did not calculate sensitivity and specificity for PE detection. Future multicenter studies with larger cohorts are needed to validate the diagnostic accuracy of this protocol. Finally, we did not evaluate the impact of this protocol on downstream clinical management or patient outcomes.

## Conclusion

In conclusion, the integration of 40 keV VMI with DLIR-H reconstruction offers an optimal solution for low-dose DE-CTPA. This protocol provides high-contrast, low-noise imaging of the pulmonary vasculature, ensuring confident assessment of segmental and subsegmental arteries while minimizing radiation and contrast burden.

## References

1. Huisman MV, Barco S, Cannegieter SC, Le Gal G, Konstantinides SV, Reitsma PH, et al. Pulmonary embolism. *Nat Rev Dis Primers* 2018;4:18028

2. Chen Q, van Rein N, Scheres LJJ, Kempers EK, Visser C, Kruip M, et al. Incidence, risk factors, and mortality of pulmonary embolism in the Netherlands (2015-22): sex differences and shifts during the coronavirus disease 2019 pandemic. *Eur Heart J* 2025;46:2809-2821

3. Yan M, Kieser R, Wu CC, Qiao W, Rojas-Hernandez CM. Clinical factors and outcomes of subsegmental pulmonary embolism in cancer patients. *Blood Adv* 2021;5:1050-1058

4. Nguyen ET, Hague C, Manos D, Memauri B, Souza C, Taylor J, et al. Canadian Society of Thoracic Radiology/Canadian Association of Radiologists Best Practice Guidance for Investigation of Acute Pulmonary Embolism, Part 2: Technical Issues and Interpretation Pitfalls. *Can Assoc Radiol J* 2022;73:214-227

5. S S, Pradhan A, Kadavigere R, Dkhar W, Sukumar S, Barnes NA, et al. Reduction of radiation dose and contrast volume in CT pulmonary angiography: A systematic review and meta-analysis. *J Med Imaging Radiat Sci* 2025;57:102140

6. Isaka Y, Hayashi H, Aonuma K, Horio M, Terada Y, Doi K, et al. Guideline on the use of iodinated contrast media in patients with kidney disease 2018. *Clin Exp Nephrol* 2020;24:1-44

7. Zhang H, Long J, Zhang X, Wang C, Liu X, Xu W, et al. Deep learning image reconstruction improves 40 keV virtual monoenergetic image quality in rectal cancer. *Eur J Radiol* 2026;195:112646

8. Meng C, Liu X, Wang Z, Long J, Wang C, Yang J, et al. Deep Learning Image Reconstruction Improves Image Quality in Dual-Low Dose Dual-Energy CT Portal Venography Compared to Adaptive Iterative Image Reconstruction Algorithm-Veo. *Acad Radiol* 2026

9. D'Angelo T, Cicero G, Mazziotti S, Ascenti G, Albrecht MH, Martin SS, et al. Dual energy computed tomography virtual monoenergetic imaging: technique and clinical applications. *Br J Radiol* 2019;92:20180546

10. Ethiraju V, Varatharajaperumal R, Arunachalam VK, KuruVambath A, Punniyakotti RS, Rajasekaran S, et al. Role of Virtual Monoenergetic Images in the Assessment of Vessel Enhancement in Segmental Level in Third-Generation Dual-Source Dual-Energy CT Pulmonary Angiography-A Prospective Study. *Indian J Radiol Imaging* 2025;35:254-262

11. Gliner-Ron M, Sosna J, Leichter I, Goldberg SN, Shaham D, Cohen D, et al. Evaluation of the Pulmonary Arteries on CTPA With Dual Energy CT: Objective Analysis and Subjective Preferences in a Multireader Study. *J Thorac Imaging* 2024;39:201-207

12. Euler A, Solomon J, Marin D, Nelson RC, Samei E. A Third-Generation Adaptive Statistical Iterative Reconstruction Technique:

Phantom Study of Image Noise, Spatial Resolution, Lesion Detectability, and Dose Reduction Potential. *AJR Am J Roentgenol* 2018;210:1301-1308

13. Koetzier LR, Mastrodicasa D, Szczykutowicz TP, van der Werf NR, Wang AS, Sandfort V, et al. Deep Learning Image Reconstruction for CT: Technical Principles and Clinical Prospects. *Radiology* 2023;306:e221257

14. Shen L, Lu J, Zhou C, Bi Z, Ye X, Zhao Z, et al. Deep learning reconstruction combined with contrast-enhancement boost in dual-low dose CT pulmonary angiography: a two-center prospective trial. *Eur Radiol* 2025;35:7225-7234

15. Kim JH, Yoon HJ, Lee E, Kim I, Cha YK, Bak SH. Validation of Deep-Learning Image Reconstruction for Low-Dose Chest Computed Tomography Scan: Emphasis on Image Quality and Noise. *Korean J Radiol* 2021;22:131-138

16. . Available at: https://www.gehealthcare.com/-/jssmedia/gehc/us/images/products/computed-tomography/truefidelity/related-content/new/truefidelity-for-gsi-whitepaper-digital-jb19879xx-final.pdf?rev=-1

17. Parakh A, Lennartz S, An C, Rajiah P, Yeh BM, Simeone FJ, et al. Dual-Energy CT Images: Pearls and Pitfalls. *Radiographics* 2021;41:98-119

18. Mohammadinejad P, Mileto A, Yu L, Leng S, Guimaraes LS, Missert AD, et al. CT Noise-Reduction Methods for Lower-Dose Scanning:

Strengths and Weaknesses of Iterative Reconstruction Algorithms and New Techniques. *Radiographics* 2021;41:1493-1508

19. Zheng Z, Ai Z, Liang Y, Li Y, Wu Z, Wu M, et al. Clinical value of deep learning image reconstruction on the diagnosis of pulmonary nodule for ultra-low-dose chest CT imaging. *Clin Radiol* 2024;79:628-636

20. Long J, Wang C, Yu M, Liu X, Xu W, Liu Z, et al. Comparison of DLIR and ASIR-V algorithms for virtual monoenergetic imaging in carotid CTA under a triple-low protocol. *Jpn J Radiol* 2025

21. Aldosari S, Sun Z. A Systematic Review of Double Low-dose CT Pulmonary Angiography in Pulmonary Embolism. *Curr Med Imaging Rev* 2019;15:453-460

22. Alobeidi H, Alshamari M, Widell J, Eriksson T, Lidén M. Minimizing contrast media dose in CT pulmonary angiography with high-pitch technique. *Br J Radiol* 2020;93:20190995

23. Davenport MS, Perazella MA, Yee J, Dillman JR, Fine D, McDonald RJ, et al. Use of Intravenous Iodinated Contrast Media in Patients With Kidney Disease: Consensus Statements from the American College of Radiology and the National Kidney Foundation. *Kidney Med* 2020;2:85-93

559

560

561

562

563 **Table 1** Patient Demographics and Scanning Parameters

| Parameter | Value |
|---|---|
| **Demographics** (*n* = 39) | |
| Age (y) | 73 (60, 77) |
| Sex | |
| Male | 19 (48.7) |
| Female | 20 (51.3) |
| BMI (kg/m $^2$) | 23.8 ± 4.3 |
| **Scanning Parameters** | |
| Scan Length (cm) | 258.6 ± 24.0 |
| $CTDI_{vol}$ (mGy) | 5.9 (5.2, 7.9) |
| DLP (mGy·cm) | 215.8 (176.7, 287.7) |
| Effective Dose (mSv) | 3.0 (2.5, 4.0) |
| Total Contrast Volume (mL) | 25.6 ± 5.3 |
| Injection Rate (mL/s) | 4.3 ± 0.9 |

564 **Note.**—Data are presented as means ± standard deviations for normally
565 distributed variables or medians with interquartile ranges in parentheses for
566 non-normally distributed variables. Numbers in parentheses for sex indicate
567 percentages.

568 BMI = body mass index; $CTDI_{vol}$ = volume CT dose index; DLP = dose-length

569 product.

570 **Table 2** Comparison of Objective Image Quality Metrics for Pulmonary Embolism

571 Across Pulmonary Vascular Regions

| Variables | 70 keV ASIR-V 50% | 40 keV ASIR-V 50% | 40 keV DLIR-M | 40 keV DLIR-H | *P*-Values |
|---|---|---|---|---|---|
| **Pulmonary Trunk (N=13)** | | | | | |
| CT Attenuation (HU) | 79.40 (67.20, 97.30) | 184.00 (124.50, 293.10) | 184.20 (129.50, 282.70) | 186.20 (133.30, 273.90) | 0.018 |
| Image Noise (SD) | 17.40 (10.20, 25.50) | 37.00 (27.70, 55.70) | 36.00 (25.60, 51.10) | 30.10 (19.40, 37.30) | 0.000 |
| SNR | 4.99 (2.64, 8.88) | 4.81 (2.00, 6.64) | 4.83 (2.88, 7.12) | 5.69 (4.01, 8.10) | 0.701 |
| CNR | 22.97 (15.67, 36.47) | 35.17 (21.44, 49.50) | 36.41 (23.63, 54.71) | 46.03 (29.97, 72.00) | 0.069 |
| **Lobular Pulmonary Artery (N=35)** | | | | | |
| CT Attenuation (HU) | 65.10 (52.05, 82.40) | 148.10 (118.45, 206.40) | 150.20 (115.95, 201.90) | 151.70 (116.00, 199.55) | < 0.001 |
| Image Noise (SD) | 13.70 (10.40, 16.55) | 37.70 (26.20, 44.85) | 34.00 (23.90, 39.80) | 28.90 (19.00, 34.00) | < 0.001 |
| SNR | 4.46 (3.38, 6.57) | 4.34 (3.08, 6.76) | 5.05 (3.55, 7.05) | 5.71 (4.34, 8.84) | 0.178 |
| CNR | 28.43 (20.26, 37.72) | 36.44 (25.77, 48.17) | 40.98 (26.37, 51.45) | 45.60 (31.38, 65.53) | 0.001 |
| **Segment Pulmonary Artery (N=27)** | | | | | |
| CT Attenuation (HU) | 60.80 (42.40, 71.30) | 179.00 (152.00, 239.30) | 176.30 (149.40, 232.20) | 178.00 (146.40, 230.95) | < 0.001 |
| Image Noise (SD) | 13.10 (10.70, 19.50) | 28.30 (23.55, 38.65) | 26.40 (22.60, 35.20) | 23.20 (18.25, 30.40) | < 0.001 |
| SNR | 4.07 (2.28, 6.29) | 5.93 (4.63, 8.23) | 6.64 (4.83, 8.87) | 8.02 (5.70, 10.26) | 0.001 |
| CNR | 27.28 (14.51, 40.04) | 32.07 (18.99, 53.05) | 39.78 (23.81, 60.63) | 52.73 (28.17, 72.87) | 0.039 |
| **Subsegment Pulmonary Artery (N=35)** | | | | | |
| Image Noise (SD) | 67.70 (45.10, 82.05) | 181.30 (107.30, 254.75) | 178.20 (114.05, 255.15) | 174.80 (117.60, 253.30) | < 0.001 |

| | | | | | |
|---|---|---|---|---|---|
| Image Noise (SD) | 14.40 (10.10, 20.75) | 32.10 (22.85, 45.15) | 28.3 (21.75, 42.80) | 22.9 (17.70, 36.50) | < 0.001 |
| SNR | 4.44 (2.77, 6.44) | 5.33 (3.01, 8.52) | 5.90 (3.35, 8.64) | 6.98 (4.26, 9.93) | 0.046 |
| CNR | 24.11 (15.91, 35.57) | 38.80 (21.08, 46.10) | 42.13 (23.69, 49.86) | 46.86 (27.88, 62.21) | 0.001 |

572 **Note.**—Data are medians, with interquartile ranges in parentheses. *P* values were
573 derived from the Kruskal-Wallis test across the four groups.
574 HU = Hounsfield unit; SD = standard deviation; SNR = signal-to-noise ratio; CNR
575 = contrast-to-noise ratio; ASIR-V = adaptive statistical iterative reconstruction-V;
576 DLIR = deep learning image reconstruction (M = medium strength, H = high
577 strength).

578 **Table 3** Comparison of Subjective Image Quality Scores Across Reconstruction
579 Protocols

| Anatomical Region / Variable | 70 keV ASIR-V 50% | 40 keV ASIR-V 50% | 40 keV DLIR-M | 40 keV DLIR-H | *P*-Value |
|---|---|---|---|---|---|
| **Pulmonary Trunk** (*n* = 13) | | | | | |
| Image Noise | 5.00 (4.00, 5.00) | 4.00 (3.00, 4.00) | 4.00 (3.50, 4.00) | 5.00 (4.50, 5.00) | < 0.001 |
| Edge Clarity | 5.00 (4.00, 5.00) | 4.00 (3.00, 4.00) | 4.00 (4.00, 4.00) | 5.00 (5.00, 5.00) | < 0.001 |
| Noise Texture | 5.00 (4.00, 5.00) | 4.00 (3.00, 4.00) | 4.00 (4.00, 4.00) | 5.00 (5.00, 5.00) | < 0.001 |
| Overall Quality | 4.50 (4.00, 5.00) | 4.00 (3.00, 4.50) | 4.00 (4.00, 4.50) | 5.00 (4.00, 5.00) | 0.021 |
| **Lobar Pulmonary Artery** (*n* = 35) | | | | | |
| Image Noise | 5.00 (4.50, 5.00) | 4.00 (3.00, 4.00) | 4.00 (3.50, 4.00) | 5.00 (4.00, 5.00) | < 0.001 |
| Edge Clarity | 5.00 (4.50, 5.00) | 4.00 (3.50, 4.00) | 4.00 (3.50, 4.75) | 5.00 (4.00, 5.00) | < 0.001 |
| Noise Texture | 5.00 (4.50, 5.00) | 4.00 (3.00, 4.00) | 4.00 (3.00, 4.00) | 5.00 (5.00, 5.00) | < 0.001 |
| Overall Quality | 5.00 (5.00, 5.00) | 5.00 (4.00, 5.00) | 5.00 (4.00, 5.00) | 5.00 (4.50, 5.00) | 0.050 |

| | | | | | |
|---|---|---|---|---|---|
| **Segmental Pulmonary Artery** (*n* = 27) | | | | | |
| Image Noise | 5.00 (5.00, 5.00) | 4.00 (3.50, 4.00) | 4.00 (3.50, 4.00) | 5.00 (4.00, 5.00) | < 0.001 |
| Edge Clarity | 5.00 (5.00, 5.00) | 4.00 (3.00, 4.25) | 4.00 (4.00, 4.50) | 4.00 (4.00, 5.00) | < 0.001 |
| Noise Texture | 5.00 (4.25, 5.00) | 4.00 (3.25, 4.00) | 4.00 (3.50, 4.00) | 4.50 (4.00, 5.00) | < 0.001 |
| Overall Quality | 5.00 (5.00, 5.00) | 4.00 (4.00, 5.00) | 4.50 (4.00, 5.00) | 5.00 (4.75, 5.00) | < 0.001 |
| **Subsegmental Pulmonary Artery** (*n* = 35) | | | | | |
| Image Noise | 5.00 (5.00, 5.00) | 4.00 (3.75, 4.00) | 4.00 (4.00, 4.00) | 5.00 (4.50, 5.00) | < 0.001 |
| Edge Clarity | 5.00 (5.00, 5.00) | 4.00 (4.00, 4.00) | 4.00 (4.00, 5.00) | 5.00 (4.75, 5.00) | < 0.001 |
| Noise Texture | 5.00 (5.00, 5.00) | 4.00 (3.75, 4.00) | 4.00 (3.75, 4.00) | 5.00 (4.00, 5.00) | < 0.001 |
| Overall Quality | 5.00 (5.00, 5.00) | 5.00 (4.00, 5.00) | 5.00 (4.00, 5.00) | 5.00 (4.50, 5.00) | < 0.001 |

**Note.**—Data are medians (interquartile ranges). Scores were assigned on a 5-point Likert scale (1 = non-diagnostic, 5 = excellent).

**Table 4** Post-hoc Pairwise Comparisons of Subjective Image Quality Metrics

| Variable | P1 | P2 | P3 | P4 | P5 | P6 |
|---|---|---|---|---|---|---|
| **Pulmonary Trunk** (*n* = 13) | | | | | | |
| Image Noise | **0.012** | **0.015** | 0.739 | 0.918 | **< 0.001** | **< 0.001** |
| Edge Clarity | **0.004** | **0.051** | 0.305 | 0.200 | **< 0.001** | **0.002** |
| Noise Texture | **0.009** | **0.016** | 0.369 | 0.663 | **< 0.001** | **< 0.001** |
| Overall Quality | 0.081 | 0.144 | 0.369 | 0.555 | **0.016** | **0.027** |
| **Lobar Pulmonary Artery** (*n* = 35) | | | | | | |
| Image Noise | **< 0.001** | **< 0.001** | 0.282 | 0.577 | **< 0.001** | **< 0.001** |

| | | | | | | |
|---|---|---|---|---|---|---|
| Edge Clarity | **< 0.001** | **< 0.001** | 0.408 | 0.267 | **< 0.001** | **0.002** |
| Noise Texture | **< 0.001** | **< 0.001** | 0.257 | 0.677 | **< 0.001** | **< 0.001** |
| Overall Quality | **0.034** | 0.144 | 0.150 | 0.549 | 0.301 | 0.756 |
| **Segmental Pulmonary Artery** (*n* = 27) | | | | | | |
| Image Noise | **< 0.001** | **< 0.001** | 0.110 | 1.000 | **0.001** | **0.001** |
| Edge Clarity | **< 0.001** | **< 0.001** | 0.085 | 0.346 | **0.001** | **0.011** |
| Noise Texture | **< 0.001** | **< 0.001** | 0.130 | 0.809 | **< 0.001** | **0.001** |
| Overall Quality | **0.001** | **0.014** | 0.522 | 0.204 | **0.004** | 0.062 |
| **Subsegmental Pulmonary Artery** (*n* = 35) | | | | | | |
| Image Noise | **< 0.001** | **< 0.001** | 0.310 | 0.716 | **< 0.001** | **< 0.001** |
| Edge Clarity | **< 0.001** | **< 0.001** | 0.622 | 0.299 | **< 0.001** | **0.005** |
| Noise Texture | **< 0.001** | **< 0.001** | 0.304 | 1.000 | **< 0.001** | **< 0.001** |
| Overall Quality | **< 0.001** | **0.002** | 0.171 | 0.171 | **0.002** | 0.075 |

**Note.**—Values are *P* values derived from post-hoc pairwise comparisons (LSD or Dunn's test). Bold values indicate statistical significance ($P < 0.050$).

**Comparisons:**

P1: 70 keV ASIR-V 50% vs. 40 keV ASIR-V 50%

P2: 70 keV ASIR-V 50% vs. 40 keV DLIR-M

**P3: 70 keV ASIR-V 50% vs. 40 keV DLIR-H (Comparison against Standard)**

P4: 40 keV ASIR-V 50% vs. 40 keV DLIR-M

**P5: 40 keV ASIR-V 50% vs. 40 keV DLIR-H (Comparison against low-dose ASIR)**

P6: 40 keV DLIR-M vs. 40 keV DLIR-H.

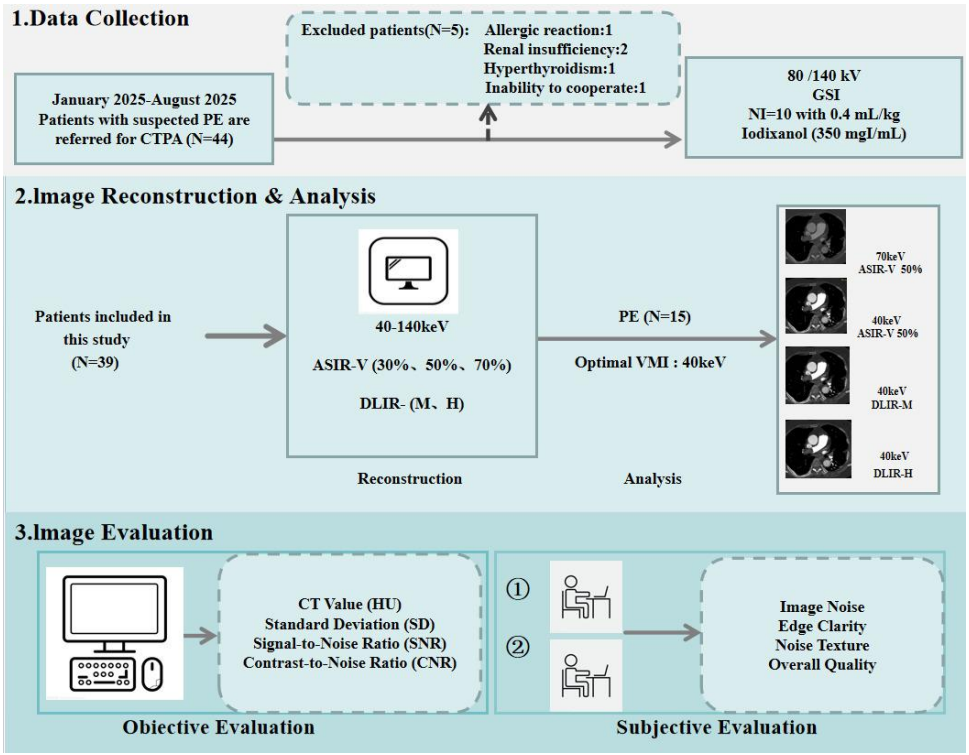



**Figure 1** Flowchart shows the study design and patient inclusion process. Patients with clinically suspected pulmonary embolism (PE) underwent dual-energy CT pulmonary angiography (CTPA) using a low-dose protocol. Image data were reconstructed at various virtual monoenergetic imaging (VMI)

levels and analyzed using both adaptive statistical iterative reconstruction-V (ASIR-V) and deep learning image reconstruction (DLIR) algorithms.

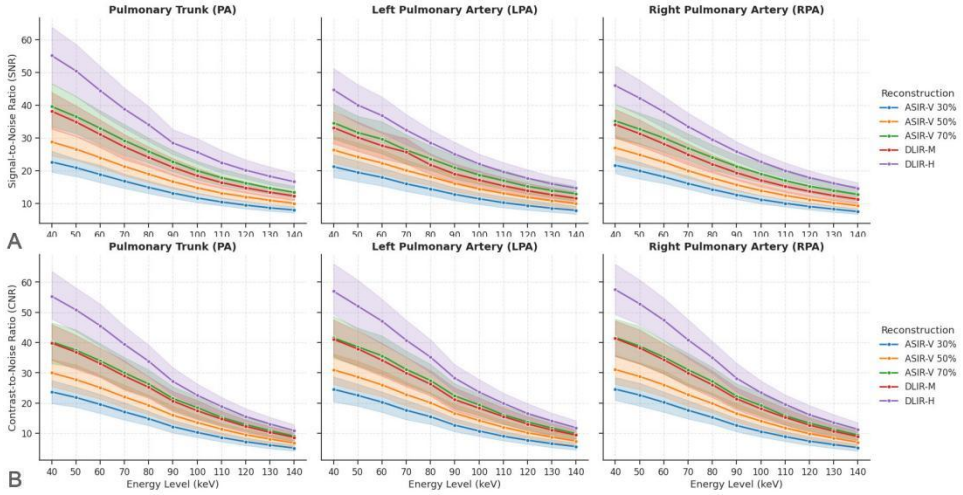



**Figure 2** Line charts illustrate the quantitative image quality metrics across virtual monoenergetic imaging (VMI) levels (40–140 keV) for five reconstruction algorithms.

**(A)** Signal-to-noise ratio (SNR) and **(B)** contrast-to-noise ratio (CNR) are stratified by anatomical region: **Pulmonary Trunk (PA)**, **Left Pulmonary Artery (LPA)**, and **Right Pulmonary Artery (RPA)**.

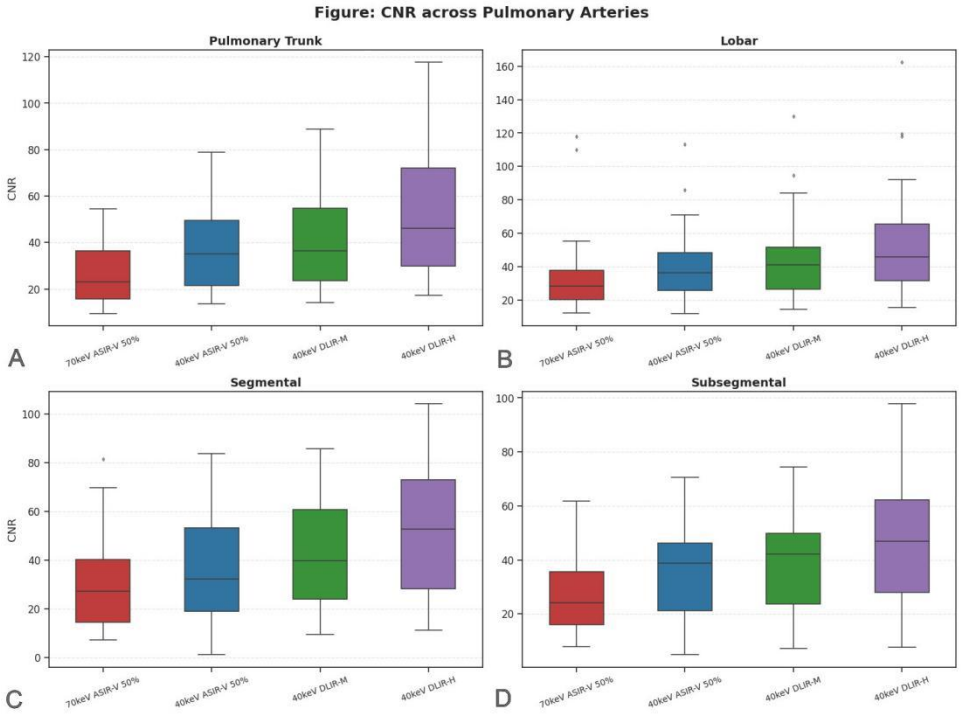



**Figure 3** Boxplots illustrate the embolus-specific contrast-to-noise ratio (CNR) across the pulmonary arterial tree.

**(A–D)** Data are stratified by anatomical region: **(A)** Pulmonary Trunk, **(B)** Lobar, **(C)** Segmental, and **(D)** Subsegmental pulmonary arteries.

**Details:** The horizontal line within each box represents the median, the box boundaries indicate the interquartile range (IQR), and the whiskers extend to the data range (excluding outliers, represented by diamonds).

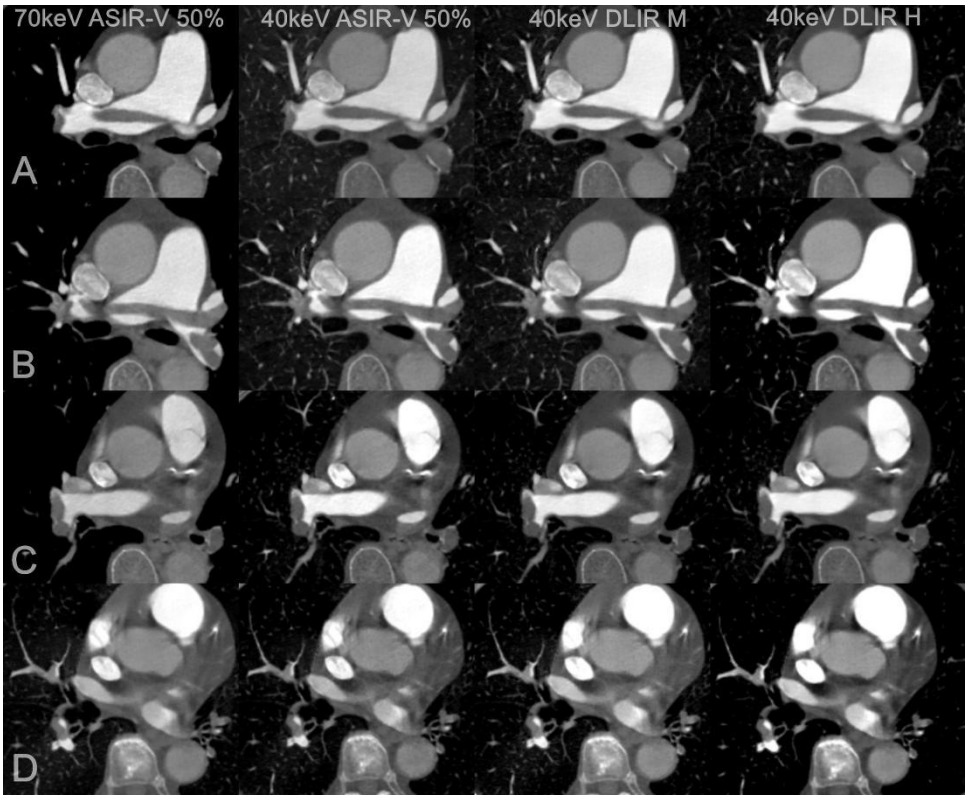



**Figure 4** Representative axial CT images comparing embolus visualization across different vascular levels and reconstruction algorithms.

**(A–D)** Images show the **(A)** pulmonary trunk, **(B)** lobar, **(C)** segmental, and **(D)** subsegmental pulmonary arteries.

**Columns:** From left to right, columns display the standard 70 keV ASIR-V 50% control, followed by 40 keV VMI reconstructions using ASIR-V 50%, DLIR-M, and DLIR-H.

## Supplementary Files

This is a list of supplementary files associated with this preprint. Click to download.

- SupplementaryInformation.pdf